Two-Dimensional Variational Mode Decomposition

Conference Paper · January 2015

DOI: 10.1007/978-3-319-14612-6_15

CITATIONS
97

READS
3,187

2 authors:

Konstantin Dragomiretskiy
Morgan Stanley
6 PUBLICATIONS **2,754** CITATIONS
SEE PROFILE

Dominique Zosso
Montana State University
43 PUBLICATIONS **3,235** CITATIONS
SEE PROFILE

Two-Dimensional Variational Mode Decomposition*

Konstantin Dragomiretskiy and Dominique Zosso

Department of Mathematics, University of California, Los Angeles
520 Portola Plaza, Box 951555, Los Angeles, CA 90095-1555, USA.
{konstantin,zosso}@math.ucla.edu

Abstract. In this paper we propose a variational method to adaptively decompose an image into few different modes of separate spectral bands, which are unknown before. A popular method for recursive one dimensional signal decomposition is the Empirical Mode Decomposition algorithm, introduced by Huang in the nineties. This algorithm, as well as its 2D extension, though extensively used, suffers from a lack of exact mathematical model, interpolation choice, and sensitivity to both noise and sampling. Other state-of-the-art models include synchrosqueezing, the empirical wavelet transform, and recursive variational decomposition into smooth signals and residuals. Here, we have created an entirely non-recursive 2D variational mode decomposition (2D-VMD) model, where the modes are extracted concurrently. The model looks for a number of 2D modes and their respective center frequencies, such that the bandlimited modes reproduce the input image (exactly or in least-squares sense). Preliminary results show excellent performance on both synthetic and real images. Running this algorithm on a peptide microscopy image yields accurate, timely, and autonomous segmentation - pertinent in the fields of biochemistry and nanoscience.

1 Introduction

In this paper we are interested in decomposing images into ensembles of constituent modes (components) that have specific directional and oscillatory characteristics. Simply put, the goal is to retrieve a small number of modes, that each have a very limited bandwidth around their characteristic center frequency. These modes are called intrinsic mode functions (IMF) and can be seen as amplitude- and frequency-modulated (AM-FM) 2D signals. Such a mode can have limited spatial support, its local (instantaneous) frequency and amplitude vary smoothly, several modes can overlap in space, and together the ensemble of modes should reconstruct the given input image up to noise and singular features.

* This work is supported by the National Science Foundation (NSF) under grant DMS-1118971, UC Lab Fees Research grant 12-LR-236660, the Swiss National Science Foundation (SNF) grant P300P2_147778, and the W. M. Keck Foundation.

The problem is inspired by the one-dimensional Empirical Mode Decomposition (EMD) algorithm [16] and its two-dimensional extensions [20, 23, 22] for recursive sifting of 2D spatial signals by means of interpolating upper and lower envelopes, median envelopes, and thus extracting image components in different "frequency" bands. This 2D-EMD, however, suffers from the same drawbacks in robustness as the original EMD in extremal point finding, interpolation of envelopes, and stopping criteria imposed.

Other methods of directional image decomposition work by mostly rigid frames, decomposing the Fourier spectrum into fixed, mostly or strictly disjoint, (quasi-)orthogonal basis elements. Examples include Gabor filters [24], wavelets [7, 18, 9], curvelets [4], shearlets [17, 14], etc. These methods are not adaptive relative to the signal, and can attribute principle components of the image to different bands, as well as contain several different image components in the same band. Adaptivity and tuned sparsity concerns have been addressed through synchrosqueezed wavelet transforms [8, 6], where unimportant wavelet coefficients are removed by thresholding based on energy content. In pursuit of the same goal, the 2D Empirical Wavelet Transform (EWT) [12, 13] decomposes an image by creating an adaptive wavelet basis.

A variational solution for the related decomposition problem in one dimension was recently presented [10]. The so-called *variational mode decomposition* in 1D is essentially based on well established concepts such as Wiener filtering, the 1D Hilbert transform and the analytic signal, and heterodyne demodulation. The goal of 1D-VMD is to decompose an input signal into a discrete number of sub-signals (modes), where each mode has limited bandwidth in spectral domain. In other words, one requires each mode k to be mostly compact around a center pulsation ω_k, which is to be determined along with the decomposition. In order to assess the bandwidth of a mode, the following scheme was proposed [10]: 1) for each mode u_k, compute the associated analytic signal by means of the Hilbert transform in order to obtain a unilateral frequency spectrum. 2) For each mode, shift the mode's frequency spectrum to "baseband", by mixing with an exponential tuned to the respective estimated center frequency. 3) The bandwidth is now estimated through the H^1 smoothness of the demodulated signal, i.e. the squared L^2-norm of the gradient. The resulting constrained variational problem is the following:

$$\begin{aligned} \min_{u_k,\omega_k} \left\{ \sum_k \alpha_k \left\| \partial_t \left[\left(\delta(t) + \frac{j}{\pi t} \right) * u_k(t) \right] e^{-j\omega_k t} \right\|_2^2 \right\} \\ \text{s.t.} \quad \forall t\colon \sum_k u_k(t) = f(t), \end{aligned} \tag{1}$$

where $*$ denotes convolution.

In this paper we propose a natural two-dimensional extension of the (1D) Variational Mode Decomposition (VMD) algorithm [10] in the context of image segmentation and directional decomposition. 2D-VMD is a non-recursive, fully

adaptive, variational method which sparsely decomposes images in a mathematically well-founded manner with minimal parameters and no explicit interpolation. Practicable applications include the decomposition of images into (possibly overlapping) regions of essentially wave-like nature, in order to make these components accessible for further analysis, such as space-frequency analysis and demodulation.

The rest of this paper is organized as follows: Section 2 presents and explains the two dimensional model. 2D generalizations of the Hilbert transform and the analytic signal are discussed. Once all of the tools from the 1D model are made analogous, we first present the constrained 2D model, and then its unconstrained formulation. The details of the optimization with respect to each unknown are shown, leading to the algorithmic updates of the variables. Section 3 contains our experiments and results, namely of two images, one synthetic multi-mode image and one real β-sheet microscopy image. We present the 2D-VMD algorithm's decomposition of these images, along with the reconstruction. Section 4 concludes on our proposed 2D-VMD method, summarizes again the main assumptions and limitations, and includes some future directions and expected improvements.

2 2D Variational Mode Decomposition

We design the 2D model relatively analogous to its 1D predecessor, minimizing the constituent sub-signals bandwidth while maintaining data fidelity. While derivatives in higher dimensions are simply generalized by gradients, and modulation is also straightforward, the generalization of the analytic signal is less obvious. To complete the analogy, we must first define the Hilbert transform along with the analytic signal in the 2D context.

2.1 2D Analytic Signal

In 1D, in the time domain, the analytic signal was achieved by adding the Hilbert transformed copy of the original signal as imaginary part:

$$f_{AS}(t) = f(t) + j\mathcal{H}\{f\}(t), \tag{2}$$

where the 1D Hilbert transform is defined as:

$$\mathcal{H}\{f\}(t) := \left\{ \frac{1}{\pi \cdot} * f(\cdot) \right\}(t) = \frac{1}{\pi} \text{p.v.} \int_{\mathbb{R}} \frac{f(v)}{t-v} dv. \tag{3}$$

We take note that the real signal is recovered simply by taking the real component of the analytic signal.

In the spectral domain, the analytic signal is obtained by suppressing the negative frequencies, thus giving it a unilateral spectrum:

$$\hat{f}_{AS}(\omega) = \begin{cases} 2\hat{f}(\omega), & \text{if } \omega > 0 \\ \hat{f}(\omega), & \text{if } \omega = 0 \\ 0, & \text{if } \omega < 0. \end{cases} \tag{4}$$

Single-sidedness of the analytic signal spectrum was the key-property motivating its use in the 1D case, since this property allowed for easy frequency shifting to base-band by complex exponential mixing. Therefore, to mimic this spectral property in 2D, one half-plane of the frequency domain must effectively be set to zero; this half-plane is chosen relative to a vector, in our case to $\boldsymbol{\omega}_k$. Thus the 2D analytic signal of interest can first be defined in the frequency domain.

$$\begin{aligned}\hat{u}_{AS,k}(\boldsymbol{\omega}) &= \begin{cases} 2\hat{u}_k(\boldsymbol{\omega}), & \text{if } \langle \boldsymbol{\omega}, \boldsymbol{\omega}_k \rangle > 0 \\ \hat{u}_k(\boldsymbol{\omega}), & \text{if } \langle \boldsymbol{\omega}, \boldsymbol{\omega}_k \rangle = 0 \\ 0, & \text{if } \langle \boldsymbol{\omega}, \boldsymbol{\omega}_k \rangle < 0 \end{cases} \\ &= (1 + \operatorname{sgn}(\langle \boldsymbol{\omega}, \boldsymbol{\omega}_k \rangle)\hat{u}_k(\boldsymbol{\omega}) \end{aligned} \tag{5}$$

The 2D analytic signal with the aforementioned Fourier property is [3]:

$$u_{AS,k}(\boldsymbol{x}) = u_k(\boldsymbol{x}) * \Big(\delta(\langle \boldsymbol{x}, \boldsymbol{\omega}_k \rangle) + \frac{j}{\pi \langle \boldsymbol{x}, \boldsymbol{\omega}_k \rangle}\Big)\delta(\langle \boldsymbol{x}, \boldsymbol{\omega}_{k,\perp} \rangle), \tag{6}$$

where $*$ denotes convolution and the transform is separable. Here, the analytic signal is calculated line-wise along the direction of reference, $\boldsymbol{\omega}_k$. These lines are processed independently, hence this definition is intrinsically 1D, but has the desired 2D Fourier property.

2.2 2D-VMD Functional

We are now able to put all the generalized VMD-ingredient together to define the two-dimensional extension of variational mode decomposition. The functional to be minimized, stemming from this definition of 2D analytic signal, is:

$$\min_{u_k, \boldsymbol{\omega}_k} \left\{ \sum_k \alpha_k \left\| \nabla \left[u_{AS,k}(\boldsymbol{x}) e^{-j\langle \boldsymbol{\omega}_k, \boldsymbol{x} \rangle} \right] \right\|_2^2 \right\} \quad \text{s.t.} \quad \forall \boldsymbol{x} \colon \sum_k u_k(\boldsymbol{x}) = f(\boldsymbol{x}) \tag{7}$$

The objective function is an assessment of the sum of the modes' bandwidths as the squared H^1 norm of its directional 2D analytic signal with only half-space frequencies, shifted to baseband by mixing with a complex exponential of the current center frequency estimate, while maintaining reconstructive signal fidelity.

The reconstruction constraint is addressed through quadratic penalty and Lagrangian multiplier, and we proceed by ADMM for optimization [10, 1, 19].

2.3 ADMM Optimization of 2D-VMD

To render the problem unconstrained, we include both a quadratic penalty and a Lagrangian multiplier to enforce the constraint fidelity; the augmented La-

grangian is now:

$$\mathcal{L}(\{u_k\},\{\omega_k\},\lambda) := \sum_k \alpha_k \left\| \nabla \left[u_{AS,k}(\boldsymbol{x}) e^{-j\langle \boldsymbol{\omega}_k, \boldsymbol{x}\rangle} \right] \right\|_2^2 + \left\| f(\boldsymbol{x}) - \sum_k u_k(\boldsymbol{x}) \right\|_2^2 + \left\langle \lambda(\boldsymbol{x}), f(\boldsymbol{x}) - \sum_k u_k(\boldsymbol{x}) \right\rangle. \quad (8)$$

Our unconstrained problem is then:

$$\min_{u_k, \boldsymbol{\omega}_k} \max_{\lambda} \mathcal{L}(\{u_k\},\{\boldsymbol{\omega}_k\},\lambda) \quad (9)$$

The solution to the original constrained minimization problem (7) is now found as the saddle point of the augmented Lagrangian $\mathcal{L}$ in a sequence of iterative sub-optimizations called alternate direction method of multipliers (ADMM) [15, 21, 2], see Algorithm 1.

For simplified notation, we incorporate the Lagrangian multiplier term λ into the quadratic penalty term, and rewrite the objective expression slightly different:

$$\sum_k \alpha_k \left\| \nabla \left[u_{AS,k}(\boldsymbol{x}) e^{-j\langle \boldsymbol{\omega}_k, \boldsymbol{x}\rangle} \right] \right\|_2^2 + \left\| f(\boldsymbol{x}) - \sum_k u_k(\boldsymbol{x}) + \frac{\lambda(\boldsymbol{x})}{2} \right\|_2^2 - \left\| \frac{\lambda(\boldsymbol{x})^2}{4} \right\|_2^2 \quad (10)$$

Minimization w.r.t. the modes u_k The relevant update problem derived from (10) is

$$u_k^{n+1} = \arg\min_{u_k} \left\{ \alpha_k \left\| \nabla [u_{AS,k}(\boldsymbol{x}) e^{-j\langle \boldsymbol{\omega}_k, \boldsymbol{x}\rangle}] \right\|_2^2 + \left\| f(\boldsymbol{x}) - \sum_i u_i(\boldsymbol{x}) + \frac{\lambda(\boldsymbol{x})}{2} \right\|_2^2 \right\}. \quad (11)$$

Since we are dealing with L^2-norms, the functional, including the augmented Lagrangian, can be written in Fourier domain utilizing the L^2 Fourier isometry:

$$\hat{u}_k^{n+1} = \arg\min_{\hat{u}_k} \left\{ \alpha_k \left\| j\boldsymbol{\omega} \left[\hat{u}_{AS,k}(\boldsymbol{\omega} + \boldsymbol{\omega}_k) \right] \right\|_2^2 + \left\| \hat{f}(\boldsymbol{\omega}) - \sum_i \hat{u}_i(\boldsymbol{\omega}) + \frac{\hat{\lambda}(\boldsymbol{\omega})}{2} \right\|_2^2 \right\} \quad (12)$$

$$= \arg\min_{\hat{u}_k} \left\{ \alpha_k \left\| j(\boldsymbol{\omega} - \boldsymbol{\omega}_k) \hat{u}_{AS,k}(\boldsymbol{\omega}) \right\|_2^2 + \left\| \hat{f}(\boldsymbol{\omega}) - \sum_i \hat{u}_i(\boldsymbol{\omega}) + \frac{\hat{\lambda}(\boldsymbol{\omega})}{2} \right\|_2^2 \right\}. \quad (13)$$

These equalities are justified by the well-known transform pair:

$$f(\boldsymbol{x}) e^{-j\langle \boldsymbol{\omega}_0, \boldsymbol{x}\rangle} \overset{\mathcal{F}}{\longleftrightarrow} \hat{f}(\boldsymbol{\omega}) * \delta(\boldsymbol{\omega} + \boldsymbol{\omega}_0) = \hat{f}(\boldsymbol{\omega} + \boldsymbol{\omega}_0), \quad (14)$$

where δ is the Dirac distribution and $*$ denotes convolution. Thus, multiplying an analytic signal with a pure exponential results in simple frequency shifting.

Taking the first variation with respect to $\hat{u}_k$ and setting it to 0 yields[1]:

$$2\alpha_k|\boldsymbol{\omega}-\boldsymbol{\omega}_k|^2\hat{u}_k + (-1)\left(\hat{f}(\boldsymbol{\omega}) - \sum_i \hat{u}_i(\boldsymbol{\omega}) + \frac{\hat{\lambda}(\boldsymbol{\omega})}{2}\right) = 0,$$
$$\forall \boldsymbol{\omega} \in \Omega_k \colon \Omega_k = \{\boldsymbol{\omega} \mid \langle \boldsymbol{\omega}, \boldsymbol{\omega}_k\rangle \geq 0\}. \quad (15)$$

With this optimality condition, solving for $\hat{u}_k$ yields the following Wiener-filter update:

$$\hat{u}_k^{n+1}(\boldsymbol{\omega}) = \Big(\hat{f}(\boldsymbol{\omega}) - \sum_{i\neq k} \hat{u}_i(\boldsymbol{\omega}) + \frac{\hat{\lambda}(\boldsymbol{\omega})}{2}\Big)\frac{1}{1+2\alpha_k|\boldsymbol{\omega}-\boldsymbol{\omega}_k|^2}$$
$$\forall \boldsymbol{\omega} \in \Omega_k \colon \Omega_k = \{\boldsymbol{\omega} \mid \langle \boldsymbol{\omega}, \boldsymbol{\omega}_k\rangle \geq 0\}, \quad (16)$$

and the other half-plane is completed through Hermitian symmetry. The term in parentheses is the signal's kth residual, where

$$\hat{f}(\boldsymbol{\omega}) - \sum_{i\neq k} \hat{u}_i(\boldsymbol{\omega})$$

is the explicit current residual, and $\hat{\lambda}_k$ accumulates the residual in the form of the Lagrangian multiplier.

Minimization w.r.t. the center frequencies $\boldsymbol{\omega_k}$ Optimizing for $\boldsymbol{\omega}_k$ is even simpler. Indeed, the update goal is

$$\boldsymbol{\omega}_k^{n+1} = \arg\min_{\boldsymbol{\omega}_k}\left\{\alpha_k \left\|\nabla\left[u_{AS,k}(\boldsymbol{x})e^{-j\langle\boldsymbol{\omega}_k,\boldsymbol{x}\rangle}\right]\right\|_2^2\right\}. \quad (17)$$

Or, again in the Fourier domain:

$$\boldsymbol{\omega}_k^{n+1} = \arg\min_{\boldsymbol{\omega}_k}\left\{\alpha_k \left\|j(\boldsymbol{\omega}-\boldsymbol{\omega}_k)\left[(1+\operatorname{sgn}(\langle\boldsymbol{\omega}_k,\boldsymbol{\omega}\rangle))\hat{u}_k(\boldsymbol{\omega})\right]\right\|_2^2\right\} \quad (18)$$
$$= \arg\min_{\boldsymbol{\omega}_k}\left\{4\alpha_k \left\|(\boldsymbol{\omega}-\boldsymbol{\omega}_k)\hat{u}_k(\boldsymbol{\omega})\right\|_{\Omega_k}^2\right\}. \quad (19)$$

The minimization is solved by letting the first variation w.r.t. $\boldsymbol{\omega}_k$ vanish (on the frequency halfplane Ω_k):

$$8\alpha_k \int_{\Omega_k} (\boldsymbol{\omega}-\boldsymbol{\omega}_k)|\hat{u}_k|^2 d\boldsymbol{\omega} = 0. \quad (20)$$

[1] Note that the functional is complex valued so the process of "taking the first variation" is not self-evident. However, the functional is analytic and complex-valued equivalents to the standard derivatives do indeed apply.

The resulting solutions are the first moments of the mode's power spectrum $|\hat{u}_k(\boldsymbol{\omega})|^2$ on the half-plane Ω_k:

$$\boldsymbol{\omega}_k^{n+1} = \frac{\int_{\Omega_k} \boldsymbol{\omega} |\hat{u}_k(\boldsymbol{\omega})|^2 d\boldsymbol{\omega}}{\int_{\Omega_k} |\hat{u}_k(\boldsymbol{\omega})|^2 d\boldsymbol{\omega}}. \tag{21}$$

Maximization w.r.t. the Lagrangian multiplier $\boldsymbol{\lambda}$ Maximizing the λ is the simplest step in the algorithm. The first variation for λ is just the data residual, $f(\boldsymbol{x}) - \sum_k u_k^{n+1}(\boldsymbol{x})$. We use a standard gradient ascent with fixed time step τ to achieve this maximization:

$$\lambda^{n+1}(\boldsymbol{x}) = \lambda^n(\boldsymbol{x}) + \tau \left(f(\boldsymbol{x}) - \sum_k u_k^{n+1}(\boldsymbol{x}) \right). \tag{22}$$

Note that the linearity of the Euler-Lagrange equation allows an impartial choice in which space to update the Lagrangian multiplier, either in the time domain or in the frequency domain. In our implementation, we perform our dual ascent update in the frequency domain, see Algorithm 1.

2.4 Optimization Algorithm

The full algorithm is detailed in Algorithm 1.

3 Experiments and Results

We have implemented the 2D-VMD method in MATLAB®[2], and test the algorithm on both a synthetic and a real image.

3.1 Synthetic Image

The first, synthetic image is a composition of spatially overlapping basic shapes, more precisely six ellipses and a rectangle, with frequency patterns varying in both periodicity and direction, courtesy of J. Gilles [11]. The spectrum is ideal for segmentation due to modes being deliberately both well isolated and narrow-banded. The resolution of the synthetic image is 256x256 and the experiment was run with parameters $\alpha = 1000$ and $K = 5$. This experiment converged in 520 iterations which took 45 seconds on a standard PC. The algorithm has no problems in accuracy nor timeliness in segmenting the image into its five constituent sub-images. The first is the DC component of the image - a solid ellipse and rectangle, while the four remaining decompositions in Fig. 1 show clear separation of the patterned ellipses. Due to the solid pieces having sharp edges, their spectra are not bandlimited and only smoothed versions are recovered. This is naturally paired with the two lower frequency modes picking up residual boundary artifacts of the DC component.

[2] Code is available at `http://www.math.ucla.edu/~zosso/code.html`

Algorithm 1 Complete ADMM optimization of 2D-VMD

Initialize $\{\hat{u}_k^0\}$, $\{\hat{\omega}_k^0\}$, $\hat{\lambda}^0$, $n \leftarrow 0$

repeat

$n \leftarrow n + 1$

for $k = 1 : K$ **do**

Create 2D Hilbert mask for Fourier multiplier

$$\mathcal{H}_k^{n+1}(\boldsymbol{\omega}) \leftarrow 1 + \mathrm{sgn}(\langle \boldsymbol{\omega_k^n}, \boldsymbol{\omega} \rangle) \tag{23}$$

Update $\hat{u}_{AS,k}$ for all $\boldsymbol{\omega}$ such that $\langle \boldsymbol{\omega_k^n}, \boldsymbol{\omega} \rangle \geq 0$:

$$\hat{u}_{AS,k}^{n+1}(\boldsymbol{\omega}) \leftarrow \mathcal{H}_k^{n+1}(\boldsymbol{\omega}) \left[\frac{\hat{f}(\boldsymbol{\omega}) - \sum_{i<k} \hat{u}_i^{n+1}(\boldsymbol{\omega}) - \sum_{i>k} \hat{u}_i^n(\boldsymbol{\omega}) + \frac{\hat{\lambda}^n(\boldsymbol{\omega})}{2}}{1 + 2\alpha|\boldsymbol{\omega} - \boldsymbol{\omega}_k^n|^2} \right] \tag{24}$$

Update $\boldsymbol{\omega}_k$:

$$\boldsymbol{\omega}_k^{n+1} \leftarrow \frac{\int_{\mathbb{R}^2} \boldsymbol{\omega} |\hat{u}_{AS,k}^{n+1}(\boldsymbol{\omega})|^2 d\boldsymbol{\omega}}{\int_{\mathbb{R}^2} |\hat{u}_{AS,k}^{n+1}(\boldsymbol{\omega})|^2 d\boldsymbol{\omega}} \tag{25}$$

Retrieve u_k:

$$u_k^{n+1}(\boldsymbol{x}) \leftarrow \Re\{\mathcal{F}^{-1} \hat{u}_{AS,k}^{n+1}(\boldsymbol{\omega})\} \tag{26}$$

end for

Dual ascent:

$$\hat{\lambda}^{n+1}(\boldsymbol{\omega}) \leftarrow \hat{\lambda}^n(\boldsymbol{\omega}) + \tau \left(\hat{f}(\boldsymbol{\omega}) - \sum_k \hat{u}_k^{n+1}(\boldsymbol{\omega}) \right) \tag{27}$$

until convergence: $\sum_k \|\hat{u}_k^{n+1} - \hat{u}_k^n\|_2^2 / \|\hat{u}_k^n\|_2^2 < K\epsilon$.

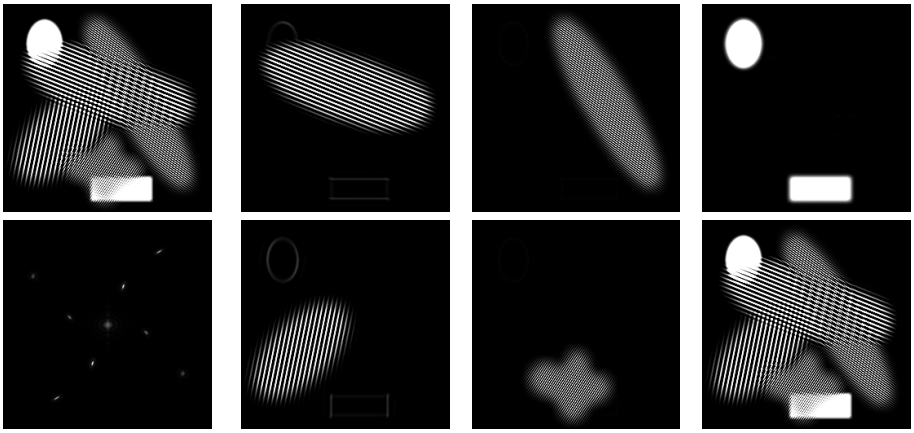

Fig. 1. Results of 2D-VMD on f_{Synth}. **Top left**: The synthetic image. **Bottom left**: Spectrum. **Right**: 5 recovered modes, and **Bottom right**: their mode superposition.

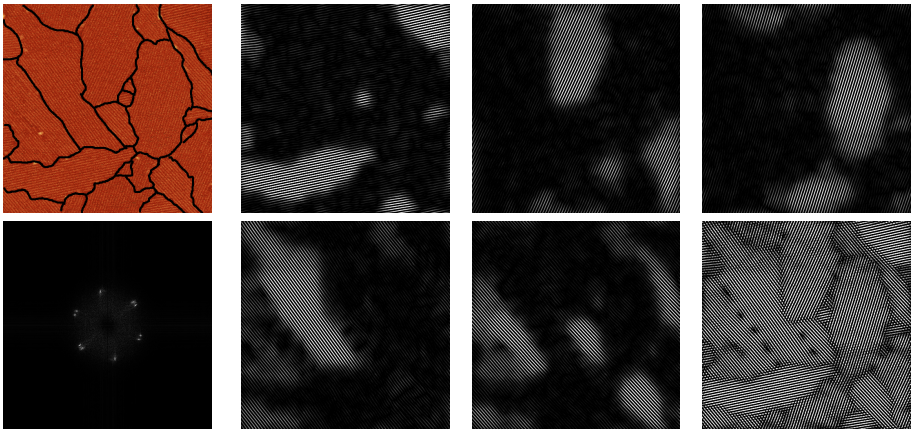

Fig. 2. Results of 2D-VMD on peptide β-sheet image. **Top left**: Peptide β-sheet (with manual boundaries), and **Bottom left**: its power spectrum. **Right**: Five recovered constituent modes, and **Bottom right**: their mode superposition.

3.2 Peptide β-sheet Microscopy Image

The second test image is a scanning tunneling microscopy (STM) image of peptide β-sheets bonding on a graphite base, courtesy of the Weiss-group at the California NanoScience Institute (CNSI), [5]. The peptide sheets grow in regions of directional homogeneity and form natural spatial boundaries where the regions meet. It is important to scientists to have accurate segmentation for their dual interests in the homogeneous regions and their boundaries. Identifying regions of homogeneity allows for the subsequent study of isolated peptide sheets of one particular bonding class. For these types of scans, manually finding the boundaries is a tedious problem that demands the attention of a skilled scientist on a rote task. In addition to speed and automation, the proposed 2D-VMD is superior in accuracy to manual boundary identification due to regions potentially having very similar patterns, varying by only a few degrees, that are difficult to discern to even the trained eye. The success of the 1D-VMD algorithm in tone separation carries over to its 2D counterpart in separating patterns that are very close, yet distinct, in spectrum.

As a common pre-processing step in image analysis, here we apply a difference-of-Gaussians (DoG) band-pass filter to the image in order to remove both noise and the DC component. Subsequently, the 2D-VMD algorithm decomposes the piecewise homogeneous peptide sheet image into its five principle components with the purpose of segmentation. Fig. 2 illustrates these individual components, and then compares their superposition to the original peptide sheet with manual boundaries added. The resolution of this peptide image is 512x512 and the experiment was run with parameters $\alpha = 5000$ and $K = 5$. This experiment converged in 210 iterations which took 140 seconds on a standard PC.

3.3 α_k Analysis and ω_k Initialization

An important degree of freedom in this algorithm is the initialization of the variables. While the u_k have a natural initialization of $u_k \equiv 0$, the $\boldsymbol{\omega}_k$ are somewhat more sensitive. Though one could manually initialize the frequencies via the image's power spectrum visualization with high accuracy, in the pursuit of full automation, we discuss the robustness of a fully unsupervised method of initialization. Qualitatively, a high α leads to finer separation of constituent subsignals due to the Wiener filter being more narrowly concentrated around its center frequency. However, this same narrow filter, if centered away from a principle frequency, may fail to capture the relevant principle frequencies. Conversely, a low α creates a wider filter, allowing the algorithm to "see and travel" to the correct frequencies, but yields worse separation. Given that we know the correct frequencies about which to initialize, a high α will produce accurate results. If we do not know estimates of the principle frequencies of the subcomponents *a priori*, it seems that we are forced to use a lower α, where the $\boldsymbol{\omega}_k$ gains freedom of mobility to the appropriate modes at the expense of proper separation. Instead of sacrificing accuracy for mobility, we keep both at the expense of computation time in the following way:

Initialize the $\boldsymbol{\omega}_k^0$ for $k = 1, ..., K$ randomly on any half-plane, such as $\{\boldsymbol{\omega} = (\omega_1, \omega_2) \mid \omega_1 \geq 0\}$. Using a high α, run the VMD algorithm and record the final values of $\boldsymbol{\omega}_k^N$. Perform this repeatedly for a number of times and create a histogram of the convergent $\boldsymbol{\omega}_k^N$, then observe the top K values. Individual iterations may converge to local minimizers, where qualitatively non-principle modes such as noise will be found, or where multiple $\boldsymbol{\omega}_k$ converge to the same principle mode while others are not picked up. The silver lining is that the non-principle convergent modes will be mostly uniformly spread across the spectrum, while the principle ones will show up with much higher consistency. This histogram of convergent modes captures the location of the consistent modes, from which we may get an excellent initialization for a final "clean" iteration. In the above peptide sheet image, we used 200 such iterations to unambiguously determine a proper initialization, though as few as 25 iterations were needed for the histogram to begin to resemble the power spectrum. Keeping this in mind, for practical applications, one can discount the ideal pursuit of automation, and do an accurate and simple graphical (semi-supervised) initialization of the frequencies to avoid multiple iterations in order to preserve timeliness.

4 Conclusions and Outlooks

In this paper, we have presented a 2D variational method for decomposing an image into an ensemble of band-limited intrinsic mode functions.

Our decomposition model solves the inverse problem as follows: decompose an image into a given number of modes such that each individual mode has limited bandwidth. We assess the mode's bandwidth as the squared H^1 norm of its directional 2D analytic signal with only half-space frequencies, shifted to baseband by mixing with a complex exponential of the current center frequency

estimate. The modes are updated by simple Wiener filtering, directly in Fourier domain with a filter tuned to the current center frequency. Then the center frequencies are updated as the center of gravity of the mode's power spectrum. We apply our model to both synthetic and real image data and can show successful decomposition.

The most important limitation of the proposed 2D-VMD is with boundary effects, and sudden signal onset in general. Despite the mostly successful decomposition, there is an issue of components' boundaries being overly smooth due to the narrow-band violation caused by discontinuous envelopes in such AM-FM signals, and a quadratic functional disfavoring and overly penalizing sharp amplitude changes, as with domain boundaries and piecewise regions. Conversely, this is also reflected by implicit periodicity assumptions when optimizing in Fourier domain. Another point is the required explicit selection of the number of active modes in the decomposition. A way to handle this issue is through the histogram method mentioned above. With many random initialization iterations, the dominant modes would show up with highest frequency, and this appropriate number of bins would become obvious by looking at an ordered distribution of the convergent frequency bins, exhibiting a gap between true frequencies and random noise. Rather than relying on iterations, both of these issues are being addressed in current work on an extended mathematical model.

We thank Paul S. Weiss and group members for sample images, and the collaborators of the W. M. Keck Foundation project "Leveraging sparsity" for inspiring discussion.

References

1. Bertsekas, D.P.: Multiplier methods: A survey. Automatica 12(2), 133–145 (1976)
2. Bertsekas, D.P.: Constrained optimization and Lagrange Multiplier methods, vol. - 1. Academic Press, Boston (1982)
3. Bülow, T., Sommer, G.: A Novel Approach to the 2D Analytic Signal. In: Computer Analysis of Images and Patterns. pp. 25–32 (1999)
4. Candes, E.J., Donoho, D.L.: Curvelets: A Surprisingly Effective Nonadaptive Representation for Objects with Edges. In: Curve and Surface Fitting. pp. 105–120 (1999)
5. Claridge, S.A., Thomas, J.C., Silverman, M.A., Schwartz, J.J., Yang, Y., Wang, C., Weiss, P.S.: Differentiating Amino Acid Residues and Side Chain Orientations in Peptides Using Scanning Tunneling Microscopy. Journal of the American Chemical Society (Nov 2013)
6. Clausel, M., Oberlin, T., Perrier, V.: The Monogenic Synchrosqueezed Wavelet Transform: A tool for the Decomposition/Demodulation of AM-FM images (Nov 2012), `http://arxiv.org/abs/1211.5082`
7. Daubechies, I.: Orthonormal bases of compactly supported wavelets. Communications on Pure and Applied Mathematics 41(7), 909–996 (Oct 1988)
8. Daubechies, I., Lu, J., Wu, H.T.: Synchrosqueezed wavelet transforms: An empirical mode decomposition-like tool. Applied and Computational Harmonic Analysis 30(2), 243–261 (Mar 2011)

9. Do, M., Vetterli, M.: Pyramidal directional filter banks and curvelets. In: Proceedings 2001 International Conference on Image Processing. vol. 2, pp. 158–161. IEEE (2001)
10. Dragomiretskiy, K., Zosso, D.: Variational Mode Decomposition. IEEE Transactions on Signal Processing 62(3), 531–544 (Feb 2014)
11. Gilles, J.: Multiscale Texture Separation. Multiscale Modeling & Simulation 10(4), 1409–1427 (Dec 2012)
12. Gilles, J.: Empirical Wavelet Transform. IEEE Transactions on Signal Processing 61(16), 3999–4010 (Aug 2013)
13. Gilles, J., Tran, G., Osher, S.: 2D Empirical Transforms. Wavelets, Ridgelets, and Curvelets Revisited. SIAM Journal on Imaging Sciences 7(1), 157–186 (Jan 2014)
14. Guo, K., Labate, D.: Optimally Sparse Multidimensional Representation Using Shearlets. SIAM Journal on Mathematical Analysis 39(1), 298–318 (Jan 2007)
15. Hestenes, M.R.: Multiplier and Gradient Methods. Journal of Optimization Theory and Applications 4(5), 303–320 (1969)
16. Huang, N.E., Shen, Z., Long, S.R., Wu, M.C., Shih, H.H., Zheng, Q., Yen, N.C., Tung, C.C., Liu, H.H.: The empirical mode decomposition and the Hilbert spectrum for nonlinear and non-stationary time series analysis. Proceedings of the Royal Society A: Mathematical, Physical and Engineering Sciences 454(1971), 903–995 (Mar 1998)
17. Labate, D., Lim, W.Q., Kutyniok, G., Weiss, G.: Sparse Multidimensional Representation using Shearlets. In: Papadakis, M., Laine, A.F., Unser, M.A. (eds.) Optics & Photonics 2005. pp. 1–9. International Society for Optics and Photonics (Aug 2005)
18. Mallat, S.: A theory for multiresolution signal decomposition: the wavelet representation. IEEE Transactions on Pattern Analysis and Machine Intelligence 11(7), 674–693 (Jul 1989)
19. Nocedal, J., Wright, S.J.: Numerical optimization. Springer, Berlin, 2nd edn. (2006)
20. Nunes, J., Bouaoune, Y., Delechelle, E., Niang, O., Bunel, P.: Image analysis by bidimensional empirical mode decomposition. Image and Vision Computing 21(12), 1019–1026 (Nov 2003)
21. Rockafellar, R.T.: A dual approach to solving nonlinear programming problems by unconstrained optimization. Mathematical Programming 5(1), 354–373 (Dec 1973)
22. Schmitt, J., Pustelnik, N., Borgnat, P., Flandrin, P.: 2D Hilbert-Huang Transform. In: Proc. Int. Conf. Acoust., Speech Signal Process (2014)
23. Schmitt, J., Pustelnik, N., Borgnat, P., Flandrin, P., Condat, L.: 2-D Prony-Huang Transform: A New Tool for 2-D Spectral Analysis p. 24 (Apr 2014), `http://arxiv.org/abs/1404.7680`
24. Tai Sing Lee: Image representation using 2D Gabor wavelets. IEEE Transactions on Pattern Analysis and Machine Intelligence 18(10), 959–971 (1996)